

The embedded cluster or association Trumpler 37 in IC 1396: a search for evolutionary constraints

T.A. Saurin^{1*}, E. Bica^{1†} and C. Bonatto^{1‡}

¹Universidade Federal do Rio Grande do Sul, Departamento de Astronomia, CP 15051, RS, Porto Alegre 91501-970, Brazil

Accepted 2012 January 12. Received 2012 January 11; in original form 2011 September 15

ABSTRACT

It is currently widely accepted that open star clusters and stellar associations result from the evolution of embedded star clusters. Parameters such as star formation efficiency, time-scale of gas removal and velocity dispersion can be determinants of their future as bound or unbound systems. Finding objects at an intermediate evolution state can provide constraints to model the embedded cluster evolution. In the H II region IC 1396, Trumpler 37 is an extended young cluster that presents characteristics of an association. We employed the Two Micron All Sky Survey (2MASS) photometry to analyse its structure and stellar content, and determine its astrophysical parameters. We also analysed 11 bright-rimmed clouds in IC 1396 in order to search for young infrared star clusters, and the background open star cluster Teutsch 74, to verify whether it has any contribution to the observed stellar density profile of Trumpler 37. The derived parameters and comparison with template objects from other studies lead us to conclude that Trumpler 37, rather than as a star cluster, will probably emerge from its molecular cloud as an OB association.

Key words: open clusters and associations: individual: Trumpler 37 – open clusters and associations: individual: Teutsch 74

1 INTRODUCTION

Studies comparing embedded and open star cluster frequencies have found that the former type is more common (e.g. Lada & Lada 2003; Bonatto & Bica 2011). The drop observed in the latter frequency has been interpreted as a result of *infant mortality*. The paradigm is that most young clusters dissolve in the field because they cannot return to dynamical equilibrium after the residual gas expulsion (Tutukov 1978; Fellhauer & Kroupa 2005; Bastian & Goodwin 2006).

A star formation efficiency (SFE – the fraction of molecular cloud gas converted into stars) higher than 50 per cent is pointed out as the main factor to determine whether a star cluster will survive an abrupt gas removal (Hills 1980). However, the observed SFE has been always less than 50 per cent (Lada & Lada 2003, and references therein). Furthermore, Kroupa (2005) showed that a single O-type star may inject, by means of winds and electromagnetic radiation, an energy higher than the cluster binding energy. This occurs on a time-scale shorter than the cluster crossing time (τ_{cr} – the time-scale over which the system as a whole will respond

to changes in the overall potential). Therefore, other parameters such as the time-scale of gas removal, tidal radius and initial cluster distribution function must play some role in this picture (Boily & Kroupa 2003). A low stellar velocity dispersion immediately before the onset of gas removal can be more important than the SFE for the cluster survival (Goodwin 2009). In addition, even a cluster with low SFE (~ 20 per cent) might survive gas removal if it has a complex structure of subclusters. Simulations by Kruijssen et al. (2011) have pointed out that the subclusters in an embedded cluster are close to virial equilibrium, and that they are weakly affected by gas removal. In this case, young clusters survive to *infant mortality* as bound systems. The merging of subclusters may form a more massive object with a much higher escape velocity (Fellhauer & Kroupa 2005). Therefore, the low efficiency formation of clusters would be the result of another disruptive process, the tidal shocks from the dense star-forming regions. Only clusters that migrate out of their natal environment in a short enough time-scale should survive.

The disruptive processes (residual gas expulsion and tidal shocks by the surrounding clouds) cause an abrupt change in the gravitational potential that may lead an embedded star cluster to endure heavy stellar loss and expand to become a stellar association. However, the stars in these unbound systems are expected to keep a common proper

* E-mail: tiago.saurin@ufrgs.br (TAS)

† E-mail: bica@if.ufrgs.br (EB)

‡ E-mail: charles@if.ufrgs.br (CB)

motion by tens of millions of years (Bastian & Goodwin 2006). Hence, distinction between star clusters (bound systems) and stellar associations may be difficult to establish for distant objects because of limitations to observe the proper motions of individual stars. Therefore, Gieles & Portegies Zwart (2011) proposed to use the ratio between stellar age and crossing time as a criterion to distinction. Thus, unbound systems would have $\text{Age}/\tau_{cr} < 1$ and bound systems, $\text{Age}/\tau_{cr} > 1$.

Examples of possible intermediate objects between embedded star clusters and stellar associations have been searched in order to determine constraints to the evolution of the embedded star clusters (e.g. Saurin, Bica & Bonatto 2010; Bonatto & Bica 2010, 2011). Evidence of dissolving clusters with escaping stars can be provided by the analysis of extensions in radial profiles for large radii reflecting changes in the gravitational potential (Bastian & Goodwin 2006).

In the present paper we analyze Trumpler 37 (Collinder 439) using the Two Micron All Sky Survey (2MASS¹; Skrutskie et al. 2006) J , H and K_S photometry and determine some astrophysical parameters that characterize this object that might be evolving to an OB association.

Trumpler 37 is embedded in the H II region IC 1396 – catalogued by Sharpless (1959) as Sh2-131 – a cloud located close to the Cep OB2 association. Fig. 1 shows a Digitized Sky Survey (DSS²; Reid et al. 1991) image of the complex. The brightest star in the complex is HR 8281 (HD 206267), a spectroscopic binary of O6.5V((f))+O9:V types that belongs to the multiple system ADS 15184 (Tokovinin 1997). This complex also includes many dark nebulae and substructures, remarkably the Elephant Trunk Nebula (IC 1396A) with many young stellar objects (e.g. Reach et al. 2004; Mercer et al. 2009). In a study by Weikard et al. (1996) about the bright-rimmed clouds in IC 1396 it was estimated a gas and dust mass $M_{cld} = 12 \times 10^3 M_{\odot}$ for the whole complex. There is some spread in the distance estimates for Trumpler 37/IC 1396, e.g. 705 pc (Becker & Fenkart 1971); 860 pc (Blitz, Fich & Stark 1982); 798 pc (Battinelli & Capuzzo-Dolcetta 1991) and 835 pc (Kharchenko et al. 2005). These values imply a mean $d_{\odot} = 800 \pm 60$ pc, which we adopt hereafter.

This paper is organised as follows. In Sect. 2 we build colour-magnitude diagrams (CMDs) and a colour-colour diagram to estimate some astrophysical parameters of Trumpler 37. In Sect. 3 we analyze the radial density profiles (RDPs) and derive structural parameters. In Sect. 4 we discuss the results and use diagnostic diagrams to compare the Trumpler 37 parameters with those of a template. In Sect. 5 we provide the concluding remarks of this work.

2 2MASS PHOTOMETRY OF TRUMPLER 37

Photometry of Trumpler 37 in the 2MASS J , H and K_S bands was extracted from the catalogue II/246 (Cutri et al. 2003) available in the VizieR³ data base (Ochsenbein et al.

2000) in a circular area of radius 350 arcmin centred on HR 8281 (Table 1 – coordinates from the SIMBAD⁴ astronomical data base; Oberto et al. 2006) for a total of 1361458 stars. As quality constraint, we only considered stars with photometric errors ≤ 0.1 mag in each band.

Fig. 2 displays $J \times (J-H)$ and $J \times (J-K_S)$ CMDs for the Trumpler 37 stellar content and field stars for an offset equal area. This is simply for comparison purposes, since the decontamination for field stars was based on a large field within the range of $r = 150-350$ arcmin, together with an outlying circular area at a distance of 13.82° and a radius of 100 arcmin centred on $\alpha = 21^{\text{h}}51^{\text{m}}00^{\text{s}}$ and $\delta = +44^{\circ}00'00''$ to improve statistics. The membership of stars of the cluster was determined by comparison of the photometric properties of the stars in the offset field and in the cluster (e.g. Bonatto & Bica 2009).

The decontamination algorithm works as follows:

(i) A spatial extraction of radius 24.5 arcmin, large enough to be statistically representative of colours and magnitude of Trumpler 37, was chosen by eye. Three-dimensional CMDs $J \times (J-H) \times (J-K_S)$ were build for this region and for the field. The step along each dimension was $\Delta J = 1.0$ and $\Delta(J-H) = \Delta(J-K_S) = 0.2$. For each cluster CMD cell we modeled the contamination based on the comparison field. Photometric uncertainties were taken into account, in the sense that what we computed was the probability of a given star to be found in a cell (this minimizes the difference of the error function between the borders of the cells). Given the probabilities of all stars, we obtained the density of stars in each cell. We carried out this procedure for the object and comparison field cells.

(ii) Subsequently, the comparison field density was converted back into an integer number of stars, which was subtracted from the cluster extraction, on a cell-by-cell basis, resulting the number of member stars in a given cell, N_{clean}^{cell} . Variations in the cell positioning corresponding to 1/3 of the adopted cell size in each dimension were allowed, such that we ran 243 different setups. Each setup produced a total number of member stars, $N_{mem} = \sum_{cell} N_{clean}^{cell}$, from which we computed the expected total number of member stars $\langle N_{mem} \rangle$ by averaging out N_{mem} over all combinations.

(iii) The stars were ranked according to the number of times they survived the 243 runs, and only the $\langle N_{mem} \rangle$ highest ranked stars were considered cluster members and transposed to the respective decontaminated CMD (bottom panels of Fig. 2). Only 2267 from the 7972 stars that were within the circle of radius 24.5 arcmin have survived the decontamination procedure. The difference between the expected number of field stars (sometimes fractional) and the number of stars effectively subtracted (integer) from each cell is the subtraction efficiency, which summed over all cells resulted 94.6 ± 0.5 per cent.

The resulting decontaminated $J \times (J-H)$ and $J \times (J-K_S)$ CMDs of Trumpler 37 are shown in Fig. 2. They reveal a prominent gap between MS and PMS stars (bottom panels in Fig. 2) even wider than that of the

¹ <http://www.ipac.caltech.edu/2mass>

² <http://cdawww.dao.nrc.ca/dss/>

³ <http://vizier.u-strasbg.fr/viz-bin/VizieR>

⁴ <http://simbad.u-strasbg.fr/simbad/>

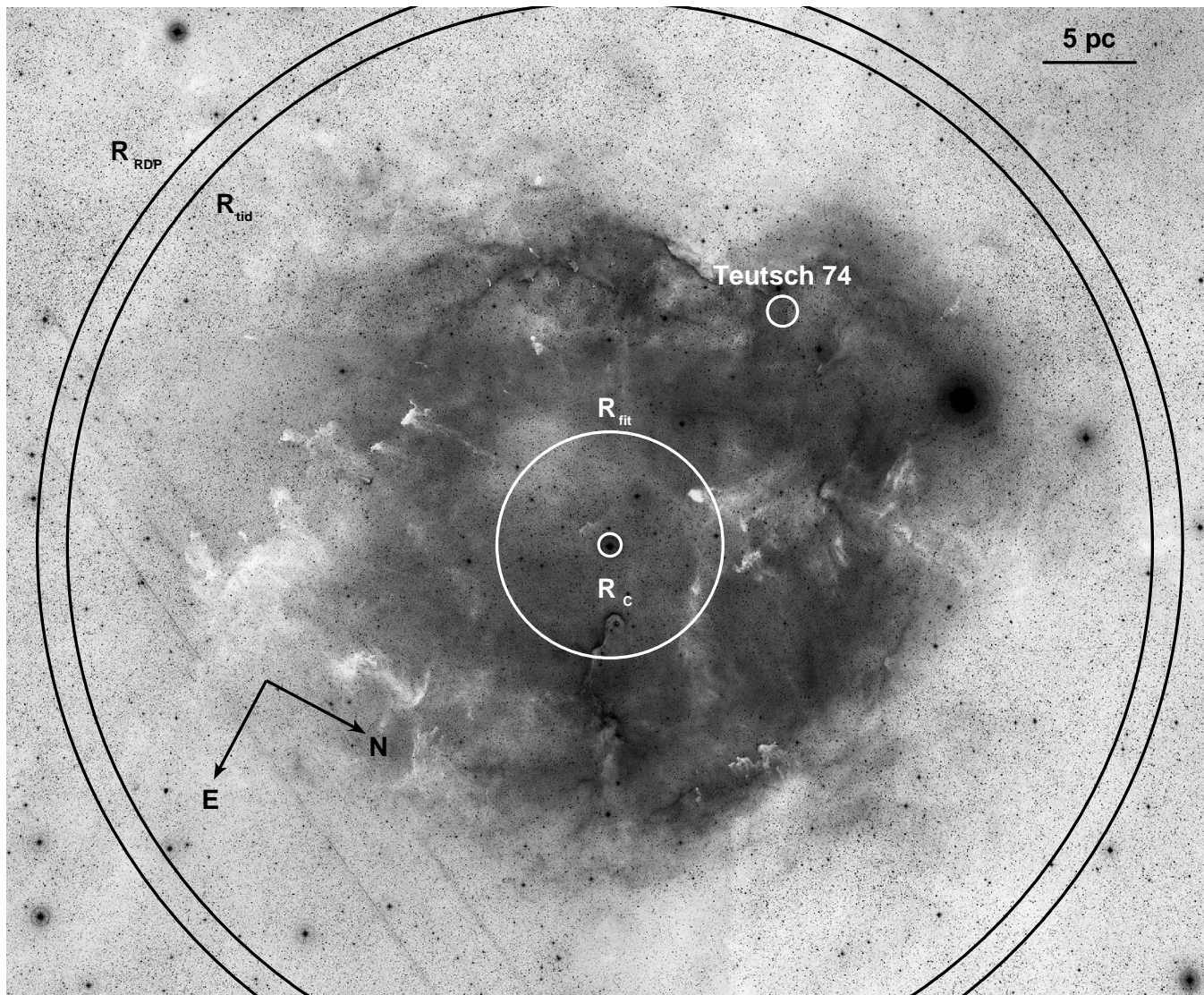


Figure 1. Combined B and R bands from DSS images with dimensions $4.3^\circ \times 3.6^\circ$ of Trumpler 37 embedded in IC 1396. Circles of radii R_c (Table 2), R_{fit} , R_{tid} and R_{RDP} (Table 3) used to analyse Trumpler 37 are indicated. The background open cluster Teutsch 74 (Sect. 3.3) is encircled in the upper right.

probable young dissolving cluster vdB 92 (Bonatto & Bica 2010).

We found that the 1 Myr Padova main-sequence (MS) isochrone (Marigo et al. 2008) and the pre-main sequence (PMS) isochrones (Siess, Dufour & Forestini 2000) for the ages 0.2, 1 and 5 Myr are the ones that best describe the sequences in the decontaminated CMDs. Since the 2MASS photometric uncertainties do not allow to detect metallicity differences, all the adopted isochrones have Solar-metallicity, suitable for the Galactic disc in general. For the purposes of this work we adopted 5 Myr as the age of Trumpler 37 (Table 1).

Morbidelli et al. (1997) estimated the absorption of fourteen bright OB stars of Trumpler 37 and suggested that the reddening towards them appears to be constant and of foreground origin. We used their mean absorption $A_V = 1.80 \pm 0.48$ mag and a distance from the Sun $d_\odot = 800$ pc (Sect. 1) as constraints to set the isochrones

(Fig. 2). We remark that in such a young cluster, the star formation process is expected to extend over a time comparable to the cluster age (e.g. Stauffer et al. 1997). Therefore, it may be very difficult to disentangle the age spread and the differential reddening, especially when photometry is the only available information (Bonatto, Bica & Lima 2011). Table 1 shows the coordinates and fundamental parameters of Trumpler 37.

We applied the relations given by Dutra, Santiago & Bica (2002) to the magnitudes of the PMS stars of our sample stars using the reddening values of Table 1 in order to build an intrinsic colour-colour diagram $(H-K_S)_0 \times (J-H)_0$ of Trumpler 37 (Fig. 3). The Classical T Tauri locus (Meyer, Calvet & Hillenbrand 1997) and the standard sequence of dwarf stars (Bessel & Brett 1988) are shown for comparison purposes. Young stellar objects of different types tend to occupy different regions in the colour-colour diagram (Lada & Adams 1992). Two

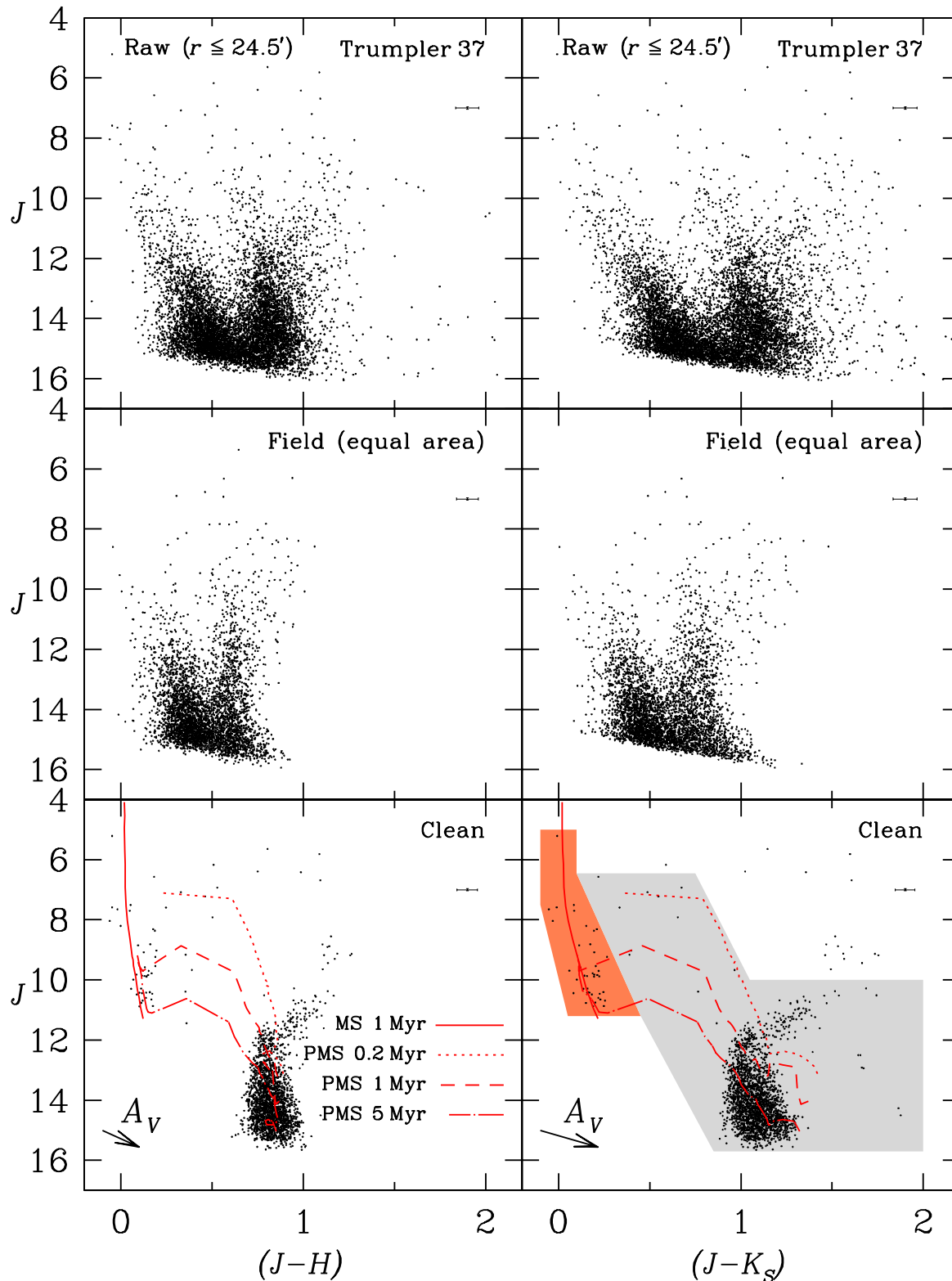


Figure 2. 2MASS colour-magnitude diagrams extracted from the $r \leq 24.5$ arcmin region of Trumpler 37. Mean uncertainties are represented by error bars in the upper right of each panel. Top panels: observed photometry with $J \times (J-H)$ (left) and $J \times (J-K_S)$ (right). Middle: equal-area extraction from the comparison field. Bottom panels: decontaminated CMDs with 1 Myr Solar-metallicity Padova isochrone (Marigo et al. 2008) and 0.2, 1 and 5 Myr PMS isochrones (Siess et al. 2000). Heavy-shaded polygon: colour-magnitude filter to isolate the MS stars. Light-shaded polygon: colour-magnitude filter for the PMS stars. The arrows indicate the reddening vectors for

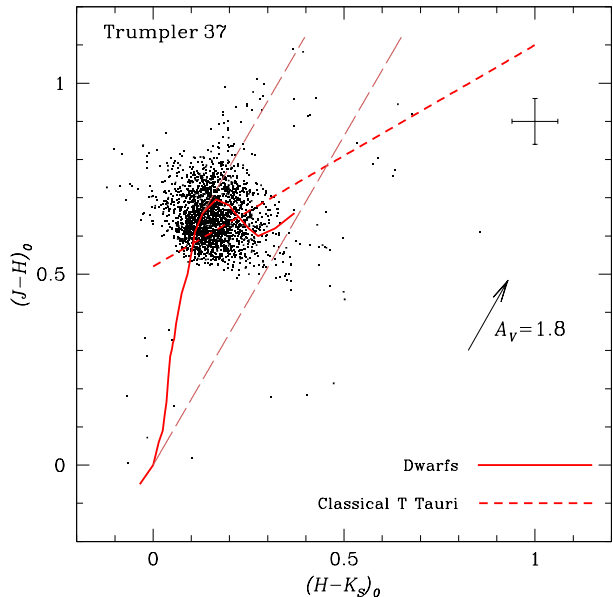


Figure 3. Extinction-corrected colour-colour diagrams $(H-K_S)_0 \times (J-H)_0$ of the PMS stars of Trumpler 37. Mean uncertainties are represented by error bars in upper right. The solid line is the standard sequence of dwarf stars (Bessel & Brett 1988) and the short-dashed line is the Classical T Tauri stars locus (Meyer et al. 1997). The arrow indicates the reddening vector for $A_V = 1.8$ mag. The two long-dashed lines define a parallel band to the reddening vector. The stars with colours that fall outside and to the right of the band have infrared excess emission, while stars that fall outside and to the left may be residual field contamination.

long-dashed lines parallel to the reddening vector are shown in Fig. 3, such that stars with colours outside and to the right of the delimiting bands are sources with infrared excess (a disk emission indicator). Herbig Ae/Be stars in general have infrared excesses larger than other young stellar objects and are located in a region delimited by $(H-K_S)_0 > 0.5$ mag and $(J-H)_0 > 0.5$ mag.

Fig. 4 shows histograms for extinction-corrected colours $(H-K_S)_0$ and $(J-H)_0$ of the PMS stars of Trumpler 37. About 33 per cent of these stars have a $(H-K_S)_0$ excess that can be attributed to residual field star contamination (Froebrich et al. 2005), but it does not affect the colour-magnitude filter limits (shaded areas in Fig. 2). The limits of these filters do not require high precision and were selected by eye. They are applied to the raw CMD within the range $r = 0' - 350'$ to minimise contamination of non-cluster stars before building the stellar RDPs (Sect. 3).

3 STELLAR DENSITY PROFILES

Since Trumpler 37 has very distinct MS and PMS populations, we define two colour-magnitude filters (shaded polygons in Fig. 2) and build separate stellar RDPs for each sequence (Fig. 5). By comparing these profiles it is possible to see a predominance of PMS stars throughout the object. A total RDP (MS + PMS) was also built (Fig. 6). All these radial profiles were built with concentric annuli and the x-axis

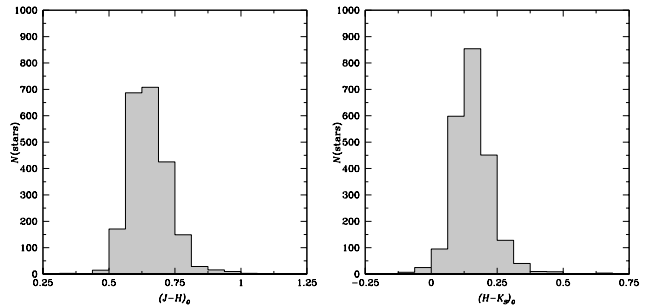


Figure 4. Distributions of the foreground extinction-corrected ($A_V = 1.8$ mag) colours of the PMS stars of Trumpler 37.

positions correspond to the most populated radial position inside each annulus.

The positions of other objects projected in the direction of Trumpler 37 are also indicated in Fig. 6. There are many dark nebulae in that region according to the catalogues VII/220A/barnard (Barnard 1927) and the VII/7A/ldn (Lynds 1962) in the Vizier data base, but for clarity we marked only some of the larger nebulae in Fig. 6.

In order to derive the structural parameters of Trumpler 37, a King-like profile (King 1962) given by

$$\Omega(r) = \Omega_{bg} + \frac{\Omega_0}{1 + (r/r_c)^2} \quad (1)$$

was fitted to the inner region (filled points in Fig. 6) of the MS and PMS composite RDP using a non-linear least-squares routine that uses the y-axis errors as weights. The structural parameters central surface density (Ω_0) and core radius (r_c) were obtained from this fit, while the background density (Ω_{bg}) was measured in a surrounding annulus in the range $r = 120' - 150'$. The cluster fitting radius (r_{fit}), defined as the projected distance from the cluster centre where the fitted curve and the background are indistinguishable, was also obtained. The values of all these parameters are shown in Tables 2-3. Fig. 1 shows a comparison between scales of the core and the fitting radii.

An estimate of the embedded mass (M_{emb}) of Trumpler 37 was made considering only the stars on the field-decontaminated CMD (Fig. 2). The mass of each MS star was determined from the corresponding mass-luminosity relation of the 1 Myr Solar-metallicity Padova isochrone (Sect. 2) using dereddened colours and magnitudes within the range $3.5 M_\odot - 40 M_\odot$. Summing the individual values, we found a total MS mass of $330_{-60}^{+10} M_\odot$. The uncertainties take into account reddening, colour excess and individual stellar mass uncertainties. Given the differential reddening, age spread and the uncertainties related to the isochrone setting, it is not possible to derive the mass of each PMS star. Consequently, we simply count the number of PMS stars and multiply it by a mean PMS stellar mass. For the latter we assumed an initial mass function of Kroupa (2001) between $0.08 M_\odot$ and $7 M_\odot$, which results in a mean mass of $0.6 M_\odot$ with a negligible uncertainty. Multiplying the number of PMS stars with infrared excess (Fig. 3) by this mean mass, yields $\sim 890 M_\odot$. Therefore, the total embedded mass inside r_{fit} is $1220_{-60}^{+10} M_\odot$. Note that these values must be considered as lower limits, owing to (i) the presence of dust, (ii) the fact that we have considered only the stars of the decon-

Table 1. Trumpler 37: fundamental parameters. By columns: (1) Galactic longitude[†]; (2) Galactic latitude[†]; (3) right ascension (J2000)[†]; (4) declination (J2000)[†]; (5) distance modulus; (6) colour excess $E(J-H)$; (7) colour excess $E(J-K_S)$; (8) colour excess $E(B-V)$; (9) V band absorption; (10) adopted age; (11) distance from the Sun; (12) Galactocentric distance considering $R_\odot = 8.4$ kpc (Reid et al. 2009). [†]Coordinates from the SIMBAD database.

l	b	α	δ	$(m-M)J$	$E(J-H)$	$E(J-K_S)$	$E(B-V)$	A_V	Age	d_\odot	d_{GC}
(1)	(2)	(3)	(4)	(5)	(6)	(7)	(8)	(9)	(10)	(11)	(12)
99° 29	3° 74	21 ^h 38 ^m 57 ^s .6	57° 29' 20'' 5	10.02±0.09	0.18±0.05	0.28±0.08	0.58±0.15	1.80±0.48	5	0.80±0.06	8.57±0.01

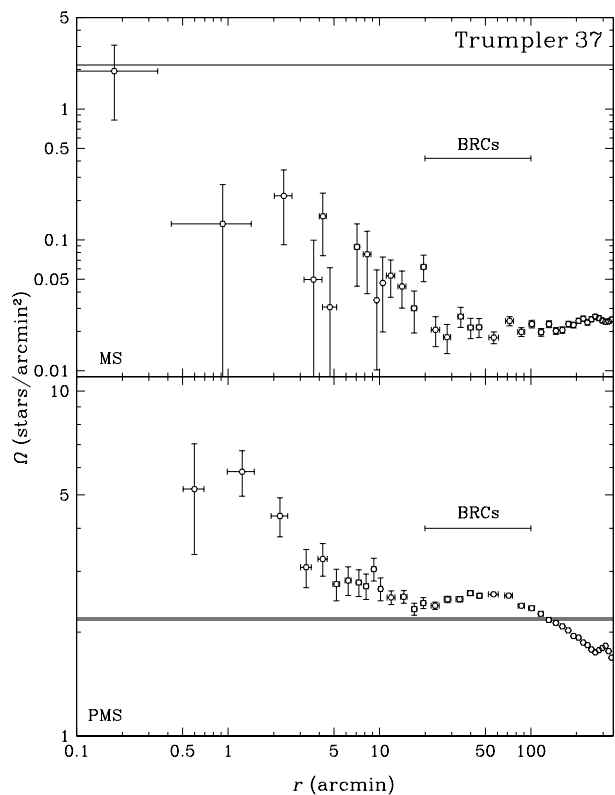


Figure 5. Stellar radial density profiles of Trumpler 37 built separately for MS (top panel) and PMS (bottom panel) with individual colour-magnitude filters (Fig. 2). Background stellar level (Table 2) with 3σ is represented by the horizontal shaded stripes. Since there are few and sparse main-sequence stars, the corresponding RDP is below the background stellar level. The BRC locus (Sect. 3.1) is indicated and it matches the bump of PMS stars in $20' \lesssim r \lesssim 100'$.

taminated CMD, (iii) the profile deviates from an isothermal sphere model (Eq. 1) for $r \gtrsim 6'$, and (iv) it has a bump beyond $r \gtrsim 20'$. The measured profile becomes statistically indistinguishable from the background at $R_{RDP} \approx 131$ arcmin (Fig. 1), this can be the intrinsic extent of Trumpler 37. In Sect. 3.1 we analyze this bump in the profile and reestimate the stellar mass of Trumpler 37.

3.1 Bright-Rimmed Clouds in IC 1396

There are 11 bright-rimmed clouds (BRCs) in IC 1396 (Sugitani et al. 1991). All of them are associated with IRAS (Infrared Astronomical Satellite) sources, presumably protostars, and may be sites of sequential star formation triggered by winds and ultra-violet radiation from nearby massive stars, mainly HR 8281.

The location of these BRCs matches the bump for $20' \lesssim r \lesssim 100$ arcmin in Figs. 5-6. In order to search for infrared subclusters we built RDPs (Fig. 7) for each BRC centred in the coordinates listed in Table 4. Since that region of IC 1396 seems to be dominated by PMS stars (Fig. 5), we selected only that population using the PMS colour-magnitude filter defined for Trumpler 37 (light-shaded polygon in Fig. 2). The restriction of photometric errors ≤ 0.1 mag in each band was removed for the stars inside a circle of radius $r \sim 0.5$ arcmin in BRC 38 and BRC 39 due to their high absorption. An inspection of the RDPs yields BRC 33, BRC 36, BRC 37, BRC 38 and BRC 39 as having profiles with relatively high central densities, suggesting small star clusters. None of them follows a King-like profile (Eq. 1).

Getman et al. (2007) and Ikeda et al. (2008) found evidence for the sequential star formation scenario in BRC 38 and BRC 37, respectively. They reported spatial gradients of stellar age along the direction to the exciting stars and detected young stellar objects in both BRC areas. The existence of these subclustering in Trumpler 37/IC 1396 resembles the hierarchical structure of NGC 346/N 66 reported by Gouliermis et al. (2008) in the Small Magellanic Cloud.

According to Getman et al. (2007), BRC 38 has a stellar mass of $\sim 15 M_\odot$. Since BRCs in IC 1396 have comparable star counts, we assume the mass of BRC 38 as representative of such subclusters. Thus, we estimate that the Trumpler 37 total embedded mass (M_{emb}) increases to $\sim 1300 M_\odot$ and its SFE is 10 per cent. This is the star formation efficiency for the whole complex. The clumps of the molecular cloud may have a higher efficiency.

3.2 Tidal radius and crossing time of Trumpler 37

Since we have an estimate of the total stellar mass in the complex, it is possible to estimate the dynamical tidal radius (r_{tid}), the distance from Trumpler 37 at which stellar motions begin to be affected by the Galaxy, from the Jacobi limit (Eq. 7-84 in Binney & Tremaine 1987) and ignoring any interaction with surrounding clouds. It can be obtained from

$$r_{tid} = \left(\frac{M}{3M_{gal}} \right)^{1/3} d_{GC}, \quad (2)$$

Table 2. Trumpler 37: structural parameters. By columns: (1) background stellar density; (2) central stellar density; (3) angular core radius; (4) linear core radius.

Ω_{bg} (stars arcmin ⁻²) (1)	Ω_0 (stars arcmin ⁻²) (2)	r_c (arcmin) (3)	R_c (pc) (4)
2.18±0.01	5.78±0.88	1.7±0.2	0.4±0.1

Table 3. Trumpler 37: scale, mass and crossing time. By columns: (1) angular fitting radius; (2) linear fitting radius; (3) velocity dispersion within the fitting radius; (4) crossing time of the fitting radius; (5) total embedded mass within the fitting radius; (6) angular tidal radius; (7) linear tidal radius; (8) angular RDP radius; (9) linear RDP radius; (10) velocity dispersion within the tidal radius; (11) crossing time of the tidal radius; (12) total embedded mass within the tidal radius; (13) star formation efficiency.

r_{fit} (arcmin) (1)	R_{fit} (pc) (2)	M_{emb}^{fit} (M _⊙) (3)	σ_V^{fit} km s ⁻¹ (4)	τ_{cr}^{fit} (Myr) (5)	r_{tid} (arcmin) (6)	R_{tid} (pc) (7)	r_{RDP} (arcmin) (8)	R_{RDP} (pc) (9)	M_{emb}^{tid} (M _⊙) (10)	σ_V^{tid} km s ⁻¹ (11)	τ_{cr}^{tid} (Myr) (12)	SFE (13)
24.4±3.7	5.7±1.0	1220 ⁺¹⁰ ₋₆₀	3.2±0.3	3.5±2	119.4±8.7	27.8±2.0	131	31	1300 ⁺¹⁰ ₋₆₀	1.4±0.1	38±22	0.1

where M_{gal} is the Galaxy mass within the Galactocentric distance d_{GC} (Table 1). We derived this mass from the relation

$$M_{gal} = \frac{V_{GC}^2 d_{GC}}{G}, \quad (3)$$

where G is the gravitational constant, and $V_{GC} = 254 \pm 16$ km/s is the circular rotation velocity in $R_{\odot} = 8.4 \pm 0.6$ kpc (Reid et al. 2009). This yields $M_{gal} \approx 10^{11} M_{\odot}$. Considering $M = M_{emb} + M_{cld}$, the tidal radius of Trumpler 37 results ~ 28 pc (~ 119 arcmin – see Fig. 1), in good agreement with the bump end associated to the BRCs.

We can also estimate the crossing time τ_{cr} by means of

$$\tau_{cr} = \frac{2R}{\sigma_V}, \quad (4)$$

where R is the cluster radius and σ_V is the stellar velocity dispersion given by

$$\sigma_V = \sqrt{\frac{GM}{R}}. \quad (5)$$

For $M = M_{emb} + M_{cld}$, with $M_{emb} = 1220 M_{\odot}$ and $R = R_{fit}$ (Sect. 3), we obtain $\tau_{cr} \approx 3.5$ Myr, slightly lower than the age of Trumpler 37. On the other hand, with $M_{emb} = 1300 M_{\odot}$ and $R = R_{tid}$, we obtain $\tau_{cr} \approx 38$ Myr. Table 3 summarizes the estimated parameters.

The comparison of the estimates of the crossing time of Trumpler 37 with its age suggests that the inner region ($r \leq R_{fit}$) may remain bound ($\text{Age} > \tau_{cr}$). On the other hand, for the whole complex ($r = R_{tid}$) we find $\text{Age} < \tau_{cr}$, which would characterize an unbound system. This difference between the two cases possibly reflects the hierarchical star formation in the molecular cloud and its fragmentation in the outer regions. This is caused by the radiation of OB stars and the tidal field of the Galaxy.

3.3 The background open cluster Teutsch 74

Teutsch 74 is an open cluster projected close to IC 1396 (Fig. 1), so it is necessary to analyze a possible contami-

nation in the Trumpler 37 photometry. For this, we used the same tools as in Sects. 2-3.

Photometry in the 2MASS J , H and K_S bands with photometric errors ≤ 0.1 mag was extracted in a circular area of radius 20 arcmin centred in the coordinates given in Table 5.

For the field star decontamination we used an annulus with $r = 10' - 20'$, where the background density (Ω_{bg}) was measured, and an outlying area of radius 100 arcmin centred on $\alpha = 21^{\text{h}}51^{\text{m}}00^{\text{s}}$ and $\delta = +44^{\circ}00'00''$ (Sect. 2). The resulting subtraction efficiency was 100 per cent. Padova isochrones of Solar-metallicity for ages of 0.5 Gyr, 1 Gyr and 2 Gyr (Marigo et al. 2008) have been set by eye to the decontaminated CMD (Fig. 8) and the fundamental parameters were derived (Table 5). Teutsch 74 appears to have a strong differential reddening, that causes a considerable spread in the CMD. We assume the age 1 Gyr of the intermediary isochrone as the approximate age of Teutsch 74.

A colour-magnitude filter was defined (shaded area in Fig. 8) and applied to the raw CMD in order to build a stellar RDP with concentric annuli. The tidal radius and mass were estimated (Table 6).

We subtracted from the Trumpler 37 photometry all the stars remaining after decontamination of Teutsch 74 (Fig. 8) and did not find any significant change in the results of the Trumpler 37 analysis.

Finally, Teutsch 74 has a stellar radial density profile (Fig. 9) that cannot be fitted by a King-like model.

4 DISCUSSION

In order to locate Trumpler 37 in an evolutionary sequence of star clusters we built diagnostic diagrams (Fig. 10) comparing its parameters to those of objects analyzed in previous studies. The comparison sample consists of:

- the structurally normal open clusters within a wide age range (70 Myr to 7 Gyr) M 26, NGC 2287, M 48, M 93, NGC 5822, NGC 3680, IC 4651, M 67 and NGC 188, plus

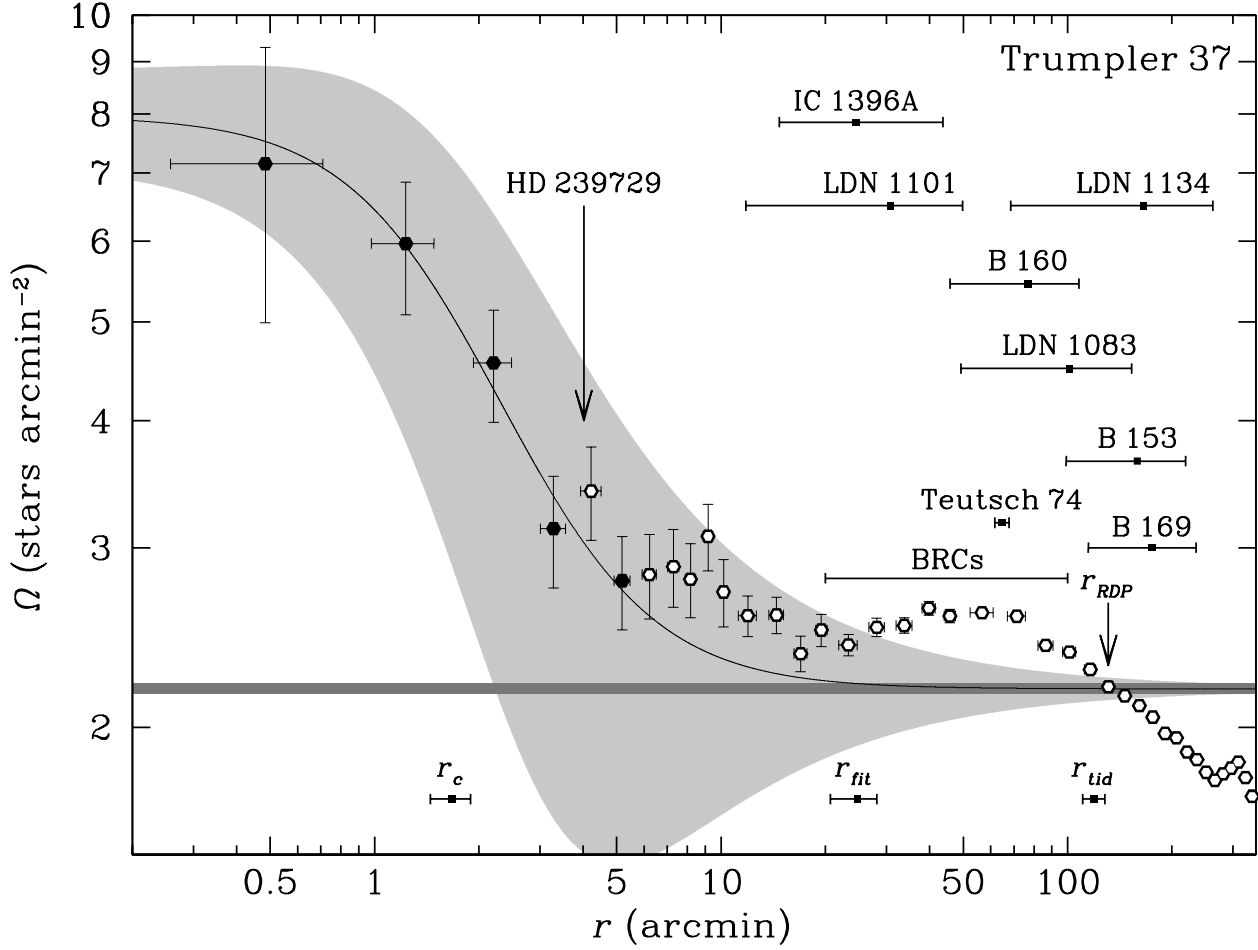


Figure 6. Total stellar radial density profile of Trumpler 37 built with both colour-magnitude filters (Fig. 2) centred on HR 8281. The King-like model (Eq. 1) fitted is shown as a solid line. Open circles were excluded from the fit. Background stellar level (Table 2) with 3σ is represented by the horizontal shaded stripe and 1σ fit uncertainty is represented by the shaded region along the fit. The core radius (r_c), fitting radius (r_{fit}), tidal radius (r_{tid}), and RDP radius (r_{RDP}) are shown. These radii are indicated in Fig. 1. The nearby projected open cluster Teutsch 74, the HD 239729 multiple star, the Elephant Trunk Nebula (IC 1396A), BRC locus (Sect. 3.1) and some surrounding dark nebulae are indicated.

Table 4. Positions determined in this study for the bright-rimmed clouds in IC 1396. By columns: (1) identification; (2) right ascension (J2000); (3) declination (J2000); (4) angular projected distance to HR 8281; (5) linear projected distance to HR 8281.

BRC	α	δ	$d_{HR\ 8281}$ (arcmin)	$D_{HR\ 8281}$ (pc)
(1)	(2)	(3)	(4)	(5)
32	21 ^h 32 ^m 34 ^s 0	57°24′27′	54.1	12.6
33	21 ^h 33 ^m 12 ^s 2	57°29′34′	48.5	11.3
34	21 ^h 33 ^m 32 ^s 4	58°03′28′	57.6	13.4
35	21 ^h 36 ^m 05 ^s 0	58°31′09′	68.7	16
36	21 ^h 36 ^m 12 ^s 4	57°27′34′	23.2	5.4
37	21 ^h 40 ^m 27 ^s 0	56°36′16′	56.7	13.2
38	21 ^h 40 ^m 43 ^s 3	58°15′40′	50.7	11.8
39	21 ^h 46 ^m 01 ^s 5	57°27′44′	59.3	13.8
40	21 ^h 46 ^m 12 ^s 6	57°09′59′	64.4	15
41	21 ^h 46 ^m 28 ^s 6	57°19′07′	64.4	15
42	21 ^h 46 ^m 35 ^s 8	57°12′15′	67	15.6

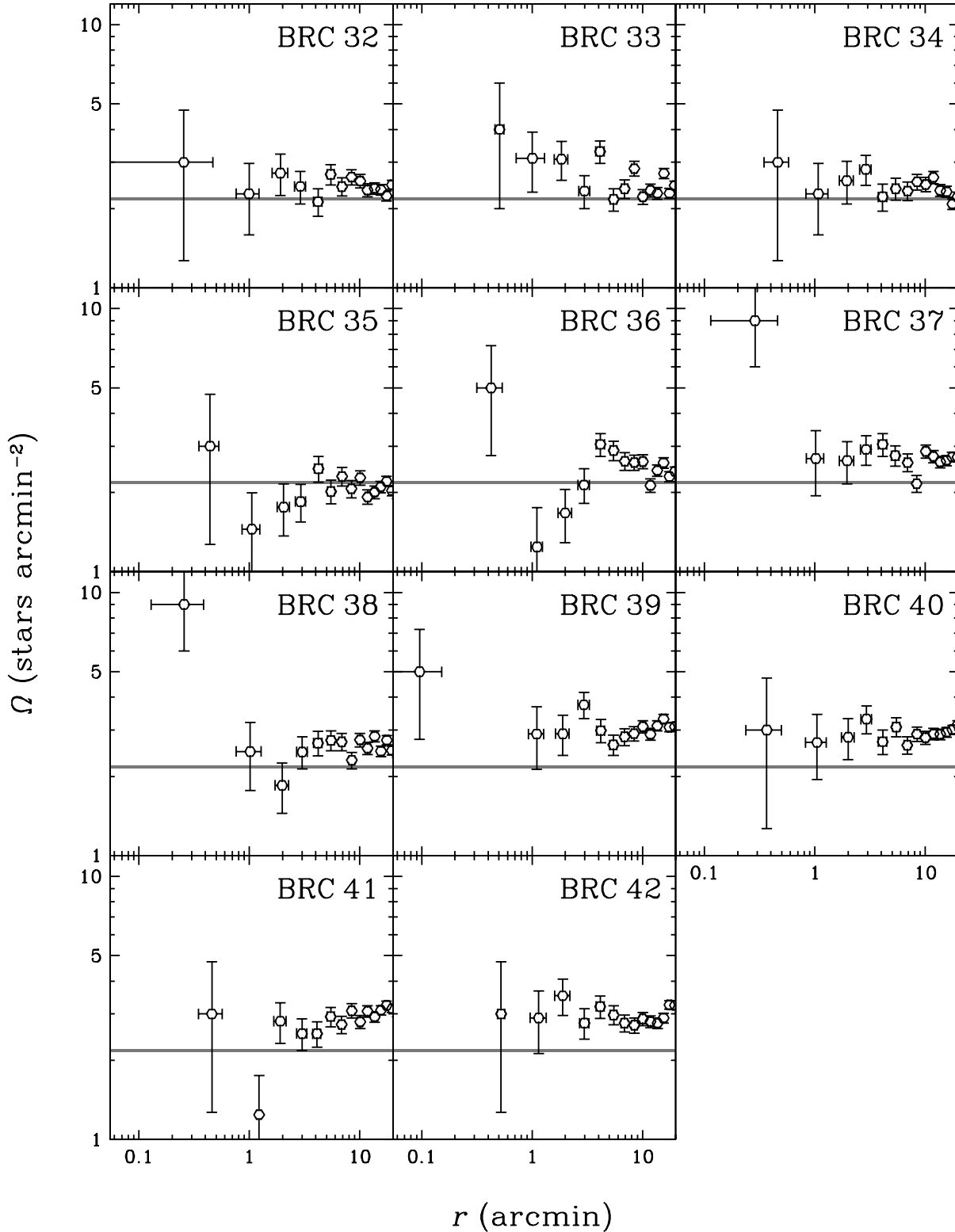


Figure 7. Stellar radial density profiles in bright-rimmed clouds in IC 1396 built with the PMS colour-magnitude filter defined for Trumpler 37 (light-shaded polygon in Fig. 2). The background stellar level (Table 2) with 3σ is represented by the narrow horizontal shaded stripes. The objects BRC 33, BRC 36, BRC 37, BRC 38 and BRC 39 have profiles with relatively high central density, suggesting small star clusters.

Table 5. Teutsch 74: fundamental parameters. By columns: (1) Galactic longitude; (2) Galactic latitude; (3) right ascension (J2000); (4) declination (J2000); (5) distance modulus; (6) colour excess $E(J-H)$; (7) colour excess $E(J-K_S)$; (8) colour excess $E(B-V)$; (9) V band absorption; (10) adopted age; (11) distance from the Sun; (12) Galactocentric distance considering $R_\odot = 8.4$ kpc (Reid et al. 2009).

l	b	α	δ	$(m-M)_J$	$E(J-H)$	$E(J-K_S)$	$E(B-V)$	A_V	Age (Gyr)	d_\odot (kpc)	d_{GC} (kpc)
(1)	(2)	(3)	(4)	(5)	(6)	(7)	(8)	(9)	(10)	(11)	(12)
100°36	3°61	21 ^h 45 ^m 40 ^s	58°05'37''	12.55±0.70	0.61±0.13	0.95±0.20	1.94±0.40	6.00±1.24	1	1.50±0.54	8.79±0.13

Table 6. Teutsch 74: scale, mass and crossing time. By columns: (1) background stellar density; (2) angular tidal radius; (3) linear tidal radius; (4) total mass inside the radius $r=3'$; (5) velocity dispersion within the tidal radius; (6) crossing time of the tidal radius.

Ω_{bg} (stars arcmin ⁻²)	r_{tid} (arcmin)	R_{tid} (pc)	M (M_\odot)	σ_V^{tid} (km s ⁻¹)	τ_{cr}^{tid} (Myr)
(1)	(2)	(3)	(4)	(5)	(6)
1.46±0.04	12.8±0.5	5.6±0.2	100±20	~0.3	39±7

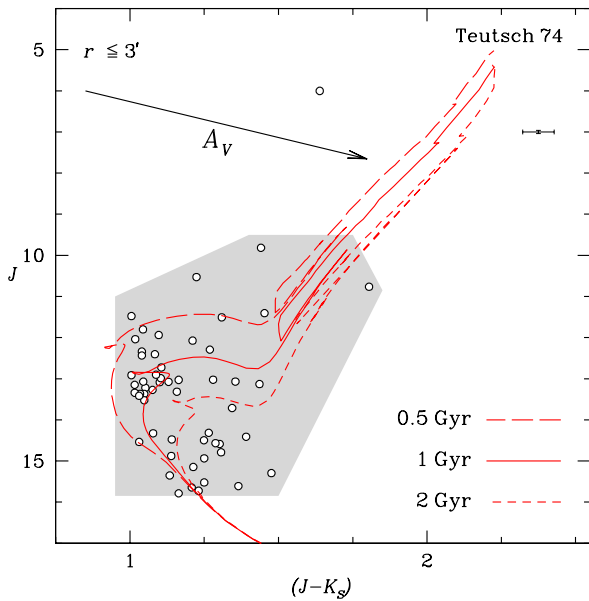


Figure 8. Decontaminated colour-magnitude diagram $J \times (J-K_S)$ extracted from the $r \leq 3$ arcmin region of Teutsch 74. Mean uncertainties are represented by error bars in upper right. Solar-metallicity Padova isochrone (Marigo et al. 2008) for ages of 0.5 Gyr (long-dashed line), 1 Gyr (solid line) and 2 Gyr (short-dashed line) are shown. The shaded polygon is a colour-magnitude filter. The arrow indicates the reddening vector for $A_V = 6.0$ mag.

the populous open clusters NGC 2477 and NGC 2516 (Bonatto & Bica 2005);

- NGC 4755, with residual stellar infrared excess emission and an age of 14 Myr (Bonatto et al. 2006);

- the very young and dynamically evolved cluster NGC 6611, with an age of 1.3 Myr (Bonatto, Santos & Bica 2006);

- Bochum 1, with an age of 9 Myr, a star cluster rem-

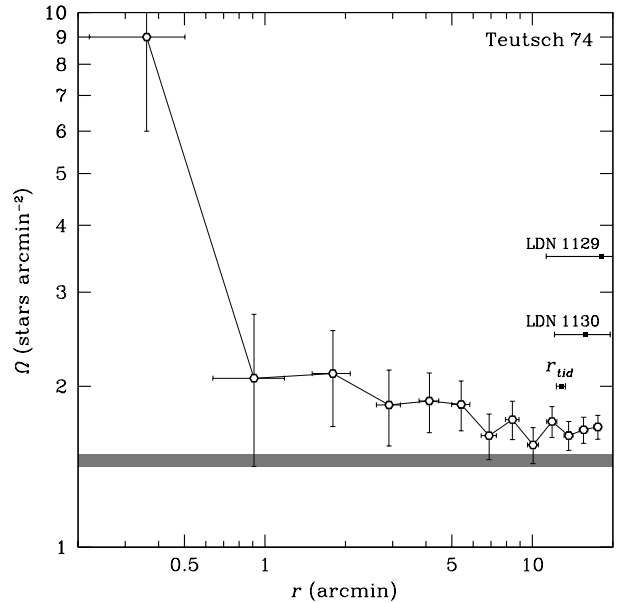


Figure 9. Stellar radial density profile of Teutsch 74 built with the colour-magnitude filter (Fig. 8). The horizontal shaded stripe is the background stellar level with 1σ (Table 6). Two dark nebulae projected in the direction of the cluster and the tidal radius (r_{tid} estimated with Eq. 2) are indicated.

nant that might be evolving into an OB association, and the bound cluster NGC 6823 with an age of 4 Myr (Bica, Bonatto & Dutra 2008);

- the dissolving young cluster NGC 2244, with an age of 3 Myr and a candidate to ordinary young open cluster NGC 2239 with an age of 5 Myr (Bonatto & Bica 2009);

- the dissolving clusters Collinder 197 and vdB 92, both with an age of 5 Myr (Bonatto & Bica 2010);

- the open cluster Teutsch 74 (Sect. 3.3);

- and Trumpler 37 itself.

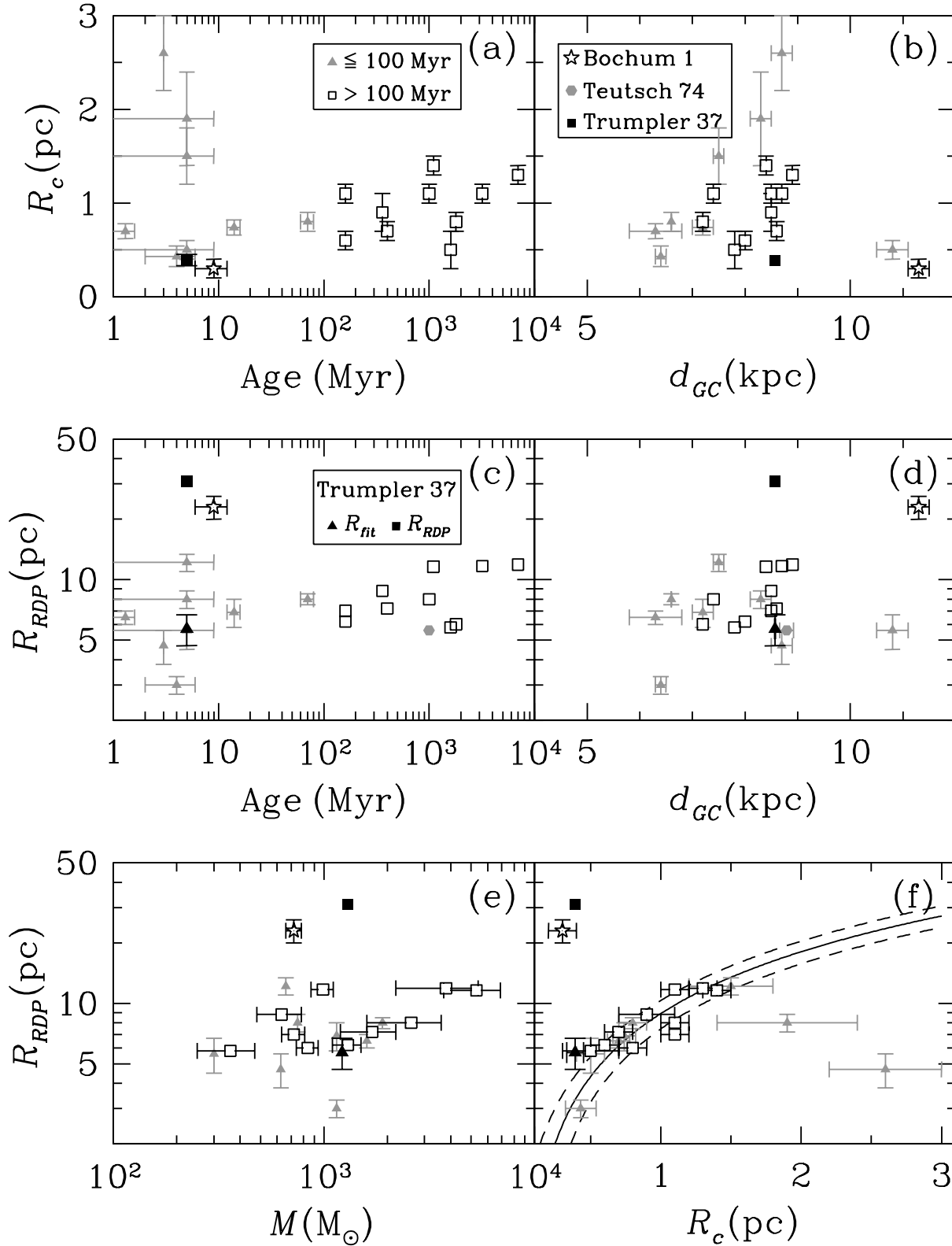


Figure 10. Diagrams comparing cluster parameters. Trumpler 37 is represented as a filled black square. When we assume $R_{RDP} = R_{fit}$, a filled black triangle represents Trumpler 37. Young clusters (≤ 100 Myr) are represented as gray triangles and old clusters (> 100 Myr) as open squares. Some error bars are smaller than the symbols. The open star represents Bochum 1, and the filled gray hexagon represents Teutsch 74. Solid line in panel (f) is a fitted curve, and dashed lines are the fitting errors. Points corresponding to Trumpler 37, Bochum 1, vdB 92 and NGC 2244 were not included in the fit.

Fig. 10, panels (a) and (b) show the dependence of the core radius on age and Galactocentric distance. Panels (c) and (d) do the same for the RDP radius. Finally, panels (e) and (f) show the dependence of the RDP radius on mass and core radius. Young clusters (≤ 100 Myr) and old clusters (> 100 Myr) are represented by different symbols.

Although the inner region of Trumpler 37 has been fitted by an isothermal model (Sect. 3), the object does not present typical parameters of a young star cluster. It has a RDP radius much larger than the fitting radius (both are represented in Fig. 1 and Fig. 10), which is larger than Bochum 1, an association that is somewhat older and more distant from the Solar circle. Thus, the extended nature of Trumpler 37 can be attributed to tidal effects and molecular cloud fragmentation. Evidence of the former process is that $R_{RDP} \approx R_{tid}$, and of the latter is that there are many BRCs in the area of Trumpler 37. Note that the RDP radius might match the tidal radius as long as Trumpler 37 is closer to the Sun (~ 730 pc) or has a larger mass ($\sim 5600 M_{\odot}$).

Panel (b) suggests a weak relation of the core radii of the clusters with the Galactocentric distances, but with a significant spread. In addition, panel (f) shows a scale relation between the RDP and core radii given by the equation $R_{RDP} = (9.16 \pm 1.06)R_c - (0.26 \pm 0.97)$, fitted with a least-squares routine with errors in both coordinates. Most objects follow this relation, except Trumpler 37, Bochum 1, vdB92 and NGC 2244 which were not included in the fit. All of them present evidence of dissolving systems. On the other hand, the inner region of Trumpler 37, delimited by the fitting radius, seems to follow this relation, so it might survive as a bound core of an expanding association.

5 CONCLUDING REMARKS

In the present paper we analyzed Trumpler 37 which is embedded in the H II region complex IC 1396. We used field-star decontaminated 2MASS photometry to build colour-magnitude diagrams and stellar radial density profiles in order to find fundamental and structural parameters. The CMD of Trumpler 37 shows a detached PMS suggesting sequential star formation and its RDP shows a core that follows a King-like model surrounded by several small subclusters with some deeply embedded stars. Trumpler 37 has a low star formation efficiency (~ 10 per cent) and $\text{Age}/\tau_{cr} < 1$, typical of objects that do not survive as bound systems. In fact, it has parameters similar to those of the objects classified as dissolving systems in previous studies. Note that these are values for the whole complex. The star formation efficiency can be higher in the clumps of the molecular cloud, and $\text{Age}/\tau_{cr} > 1$ in the inner region of Trumpler 37 which is fitted by an isothermal sphere model. Anyway, Trumpler 37 might characterize an intermediate case between an embedded cluster and an OB association.

ACKNOWLEDGMENTS

We thank an anonymous referee for interesting remarks. We acknowledge support from the Brazilian Institution CNPq. We acknowledge use of the SIMBAD database and the VizieR Catalogue Service operated at the CDS, Strasbourg,

France. This publication makes use of data products from the Two Micron All Sky Survey, which is a joint project of the University of Massachusetts and the Infrared Processing and Analysis Centre/California Institute of Technology, funded by the National Aeronautics and Space Administration and the National Science Foundation. This research used the facilities of the Canadian Astronomy Data Centre operated by the National Research Council of Canada with the support of the Canadian Space Agency.

REFERENCES

- Barnard E.E., 1927, in Catalogue of 349 dark objects in the sky, University of Chicago Press, Chicago
- Bastian N., Goodwin S.P., 2006, MNRAS, 369, L9
- Battinelli P., Capuzzo-Dolcetta R., 1991, MNRAS, 249, 76
- Becker W., Fenkart R., 1971, A&AS, 4, 241
- Bessel M.S., Brett J.M., 1988, PASP, 100, 1134
- Bica E., Bonatto C., Dutra C.M., 2008, A&A, 489, 1129
- Binney J., Tremaine S., 1987, in Galactic Dynamics, Princeton University Press, Princeton
- Blitz L., Fich M., Stark A.A., 1982, ApJS, 49, 183
- Boily C.M., Kroupa P., 2003, MNRAS, 338, 665
- Bonatto C., Bica E., 2005, A&A, 437, 483
- Bonatto C., Bica E., 2009, MNRAS, 394, 2127
- Bonatto C., Bica E., 2010, A&A, 516, 81
- Bonatto C., Bica E., 2011, MNRAS, 415, 2827
- Bonatto C., Bica E., Lima E.F., 2012, MNRAS, 420, 352
- Bonatto C., Bica E., Ortolani S., Barbuy B., 2006, A&A, 453, 121
- Bonatto C., Santos, Jr., J.F.C., Bica E., 2006, A&A, 445, 567
- Cutri R.M., Skrutskie M.F., van Dyk S., Beichman C.A., Carpenter J.M., Chester T., Cambresy L., Evans T., Fowler J., Gizis J., Howard E., Huchra J., Jarrett T., Kopan E.L., Kirkpatrick J.D., Light R.M., Marsh K.A., McCallon H., Schneider S., Stiening R., Sykes M., Weinberg M., Wheaton W.A., Wheelock S., Zacarias N., 2003, 2MASS All-Sky Catalog of Point Sources (Cutri+ 2003), VizieR Online Data Catalog, vol. 2246
- Dutra C.M., Santiago B.X., Bica E., 2002, A&A, 381, 219
- Fellhauer M., Kroupa P., 2005, ApJ, 630, 879
- Froeblich D., Scholz A., Eislöffel J., Murphy G.C., 2005, A&A, 432, 575
- Getman K.V., Feigelson E.D., Garmire G., Broos P., Wang J., 2007, ApJ, 654, 316
- Gieles M., Portegies Zwart S.F., 2011, MNRAS, 410, L6
- Goodwin S.P., 2009, Ap&SS, 324, 259
- Gouliermis D.A., Chu Y.-H., Henning T., Brandner W., Gruendl R.A., Hennekemper E., Hormuth F., 2008, ApJ, 688, 1050
- Hills J.G., 1980, ApJ, 225, 986
- Ikeda, H., Sugitani K., Watanabe M., Fukuda N., Tamura M., Nakajima Y., Pickles A.J., Nagashima C., Nagayama T., Nakaya H., Nakano M., Nagata T., 2008, AJ, 135, 2335
- Kharchenko N.V., Piskunov A.E., Roeser S., Schilbach E., Scholz R.-D., 2005, A&A, 438, 1163
- King I., 1962, AJ, 67, 471
- Kroupa P., 2001, MNRAS, 322, 231
- Kroupa P., 2005, in Turon C., O’Flaherty K.S., Perryman

- M.A.C., eds, ESA SP-576, The Three-Dimensional Universe with Gaia, ESA, Noordwijk, p. 629
- Kruijssen J.M.D., Maschberger T., Moeckel N., Clarke C.J., Bastian N. Bonnell I.A., 2011, MNRAS, 419, 841
- Lada C.J., Adams F.C., 1992, ApJ, 393, 278
- Lada C.J., Lada E.A., 2003, ARA&A, 41, 57
- Lynds B.T. 1962, ApJS, 7, 1
- Marigo P., Girardi L., Bressan A., Groenewegen M.A.T., Silva L., Granato G.L., 2008, A&A, 482, 883
- Mercer E.P., Miller J.M., Calvet N., Hartmann L., Hernandez J., Sicilia-Aguilar A., Gutermuth R., 2009, AJ, 138, 7
- Meyer M.R., Calvet N., Hillenbrand L.A., 1997, AJ, 114, 288
- Morbidelli L., Patriarchi P., Perinotto M., Barbaro G., di Bartolomeo A., 1997, A&A, 327, 125
- Oberto A., Wenger M., Lejal J.P., Jaehn S., Baranne B., Hatt M., Dellicour O., Deprez J., 2006, in Gabriel C., Arviset C., Ponz D., Enrique S., eds, ASPC, v. 351, Astronomical Data Analysis Software and Systems XV, PASP, San Francisco, p. 703
- Ochsenbein F., Bauer P., Marcout J., 2000, A&AS, 143, 23
- Reach W.T., Rho J., Young E., Muzerolle J., Fajardo-Acosta S., Hartmann L., Sicilia-Aguilar A., Allen L., Carey S., Cuillandre J.-C., Jarrett T.H., Lowrance P., Marston A., Noriega-Crespo A., Hurt R.L., 2004, ApJS, 154, 385
- Reid I.N., Brewer C., Brucato R.J., McKinley W.R., Maury A., Mendenhall D., Mould J.R., Mueller J., Neugebauer G., Phinney J., Sargent W.L.W., Schombert J., Thickett R., 1991, PASP, 103, 661
- Reid M.J., Menten K.M., Zheng X.W., Brunthaler A., Moscadelli L., Xu Y., Zhang B., Sato M., Honma M., Hirota T., Hachisuka K., Choi Y.K., Moellenbrock G.A., Bartkiewicz A., 2009, ApJ, 700, 137
- Saurin T.A., Bica E., Bonatto C., 2010, MNRAS, 407, 133
- Sharpless S., 1959, ApJS, 4, 257
- Skrutskie M.F., Cutri R.M., Stiening R., Weinberg M.D., Schneider S., Carpenter J.M., Beichman C., Capps R., Chester T., Elias J., Huchra J., Liebert J., Lonsdale C., Monet D.G., Price S., Seitzer P., Jarrett T., Kirkpatrick J.D., Gizis J.E., Howard E., Evans T., Fowler J., Fullmer L., Hurt R., Light R., Kopan E.L., Marsh K.A., McCallon H.L., Tam R., Van Dyk S., Wheelock S., 2006, AJ, 131, 1163
- Siess L., Dufour E., Forestini M., 2000, A&A, 358, 593
- Stauffer J.R., Hartmann L.W., Prosser C.F., Randich S., Balachandran S., Patten B.M., Simon T., Giampapa M., 1997, ApJ, 479, 776
- Sugitani K., Fukui Y., Ogura K., 1991, ApJSS, 77, 59
- Tokovinin A.A., 1997, A&ASS, 124, 75
- Tutukov A.V., 1978, A&A, 70, 57
- Weikard H., Wouterloot J.G.A., Castets A., Winnewisser G., Sugitani K., 1996, A&A, 309, 581